# Nonlinear dynamics of the atomic force microscope at the liquid-solid interface

Daniel Kiracofe and Arvind Raman
*School of Mechanical Engineering and Birck Nanotechnology Center, Purdue University, West Lafayette, Indiana 47907, USA*
(Received 25 August 2012; published 5 November 2012)

The measurement of intermolecular forces at the liquid-solid interface is key to many studies of electrochemistry, wetting, catalysis, biochemistry, and mechanobiology. The atomic force microscope (AFM) is unique in its ability to measure and map these forces with nanometer resolution using the oscillating sharp tip of an AFM cantilever. These surface forces are only measured by observing the changes they induce in the dynamics of the resonant AFM probe. However, AFM cantilever dynamics at this interface can be significantly different when compared to air/vacuum environments due to the nature of nanoscale forces at the interface and the low-quality factors in liquids. In this work, we study the nonlinear dynamics of magnetically excited AFM microcantilevers on graphite and mica immersed in deionized water, high-concentration buffers, and methanol. By combining theory and experiments, a wealth of nonlinear dynamical phenomena such as superharmonic resonance, hysteretic jumps, and multimodal interactions are demonstrated and their dependence on hydration/solvation forces is clarified. These results are expected to aid ongoing efforts to link liquid-solid interface properties to cantilever dynamics and lead to accurate interpretation of data from experiments.

DOI: 10.1103/PhysRevB.86.205405 PACS number(s): 68.08.De, 07.79.Lh

## I. INTRODUCTION

Dynamic atomic force microscopy (AFM) uses a resonant cantilever to probe the forces between a nanoscale tip and a sample. In recent years, advances in dynamic AFM methods have made it possible to study at high resolution the intermolecular forces associated with fundamental physical processes at liquid-solid interfaces such as the organization of solvation shells,[1] self-assembly of molecules on surfaces,[2] and electrochemistry.[3] In dynamic AFM, these intermolecular forces can only be measured through the changes they induce in the dynamics of the oscillating cantilever probe. The resulting dynamics can be nonintuitive and complex because the oscillating cantilever and the intermolecular forces form a nonlinear dynamical system. A fundamental understanding of the dynamics of this coupled system is therefore key to quantitative measurements of forces at the liquid-solid interface using dynamic AFM.

The nonlinear dynamical behavior of this system in air or vacuum environments is well known.[4] The most well-known example of this is the role of van der Waals and nanoscale repulsive interactions in the coexistence of multiple stable oscillation states of resonantly driven cantilevers in tapping mode (i.e., the attractive and repulsive regimes).[5] However, despite the increasing use of AFM in liquid environments (to measure intermolecular forces for applications in electrochemistry,[6] mechanobiology,[7] wetting,[8] etc.), the nonlinear dynamics of AFM cantilevers coupled to forces at the liquid-solid interface is relatively poorly understood. A better understanding of AFM nonlinear dynamics in liquid environments will allow users to correctly interpret their experimental data, and enable the design of AFM hardware that is better suited to the unique dynamics in liquids.

There are several key differences between ambient or vacuum environments and liquid environments that must be taken into account in understanding the nonlinear dynamical interactions between the oscillating cantilever and the intermolecular forces that characterize the liquid-solid interface. The first is the large hydrodynamic drag, which leads to low-quality factors of the cantilever resonance. Whereas the quality factor in air may be several hundred or more, in liquid it is generally less than ten, and often less than two (there are, however, a few exceptions such as Ref. 9 that use very stiff tuning forks instead of cantilevers). This was clearly observed from the earliest works on dynamic AFM in liquids,[10] but it has many subtle implications that are still not commonly understood. Analysis techniques that are accurate for high-quality factors are simply not applicable to low-quality-factor environments.

Second, the relevant types of surface forces are different. Attractive van der Waals forces and capillary forces, which can be large in ambient environments, are small or nonexistent in liquid. However, in liquids, there are two additional forces not present in ambient environments. First is the well-known electric double layer.[11] Second, when the surfaces approach to within a few molecular diameters of each other, the liquid can no longer be modeled as a continuum. Noncontinuum effects arise due to the nanoscale geometric confinement and the interaction of solvent molecules with the surface, which include solvation and hydration forces.[11,12]

There have been previous studies of various aspects of AFM operation in liquids.[13–25] However, no one study has yet to put together all of the diverse pieces into a complete understanding of cantilever dynamics in liquids. In this work, we present comprehensive experimental and theoretical studies of cantilever dynamics in liquids.

The layout of the paper is as follows: First, we review the background and prior work. Then, experimental data are presented and analyzed. The experiments are conducted with magnetic excitation, allowing a well-behaved frequency response spectrum (i.e., amplitude and phase). Next, theoretical modeling is presented, which is used to numerically simulate the nonlinear frequency response. Finally, the model is used to study the effects of various parameters and gain further insight into the causes of the nonlinear phenomena.

 

## II. BACKGROUND

Prior works in this area have broadly focused on either the tip-sample interaction forces in liquids or on understanding the dynamics of the oscillating cantilever at this interface. Of the many forces at the liquid-solid interface, the most prominent one is the electrical double layer [e.g., typically modeled using the Derjaguin, Landau, Verwey, and Overbeek (DLVO) theory[11,12]], which has been studied using AFM by many groups.[26,27] Beyond the long-range electrostatic forces, there are several distinct short-range forces that exist between surfaces in liquids.[11,12] The first of these are the solvation or oscillatory forces, which arise because the liquid molecule density fluctuates near the surface with a period equal to the molecule diameter. When the tip oscillation amplitudes are larger than molecular diameter (as is usually the case), then the oscillatory forces are averaged out and a monotonic background force can be seen. Between two hydrophillic surfaces, these background forces are generally repulsive and are often referred to as hydration forces. Between two hydrophobic surfaces, these forces are generally attractive and may simply be referred to as hydrophobic forces.[12] Hydration, hydrophobic, and solvation forces have been studied extensively with AFM. Due to the small tip radius, these forces can be mapped with nanoscale accuracy (spatial resolution $<1$ nm and force resolution $<100$ pN). With the best instruments, it is possible to discern differences in the surface forces when the tip is over different lattice sites on a mica surface, and to map the structure of the liquid in a three-dimensional volume.[1,28] Such studies are usually conducted with small cantilever amplitudes, generally $<1$ nm and in some cases $<1$ Å amplitude.[29]

Fewer works have studied the dynamics of cantilevers under the influence of these forces. Most early analysis used the same cantilever dynamics models for liquid environments as for air/vacuum, changing only the value of parameters (i.e., quality factor). Reference 14 was perhaps the first to recognize that liquid environments often require a different model. Specifically, Ref. 14 observed that when a cantilever taps on a surface, there is a distortion of the deflection waveform that is a decaying sine wave at the cantilever's second natural frequency. In other words, when the tip taps on the surface, the cantilever feels a sudden impulsive force, which momentarily excites the second eigenmode. The implication of this coupling is that data interpretation in liquid environments can be significantly more complicated than in air or vacuum environment because a multiple eigenmode model is necessary. However, the coupling can also be exploited to gain information about the sample material properties.[20–22]

Another important implication is that understanding the nonlinear dynamics of the AFM in liquids requires the observation and prediction of processes that happen over a wide frequency bandwidth. It is not sufficient to study the dynamics only at a single frequency. This is a limitation of most of the existing work on nonlinear dynamics in liquids.[13–19] Although these studies do provide insight, they show only a small slice of the entire response. The only studies of the dynamics over a wider frequency range that the authors are aware of are Refs. 23–25. Each of these studies provides insight, but no one work has yet to put together all of the diverse pieces into a comprehensive study.

Thus, in this work, we focus on understanding the nonlinear frequency response of the AFM cantilever at the liquid-solid interface over a wide bandwidth using magnetic excitation (free from piezo resonances). We analyze the results in the context of a multiple eigenmode model that includes both contact forces from a substrate as well as short-range hydration/hydrophobic forces. Detailed comparisons are presented between experiments and numerical simulations.

In the experimental work, we have limited ourselves to either high-concentration buffer solution or deionized water. In either case, the gradient of the electrical double-layer forces are small and are neglected in the theoretical simulations. Furthermore, the tip oscillation amplitudes (5 nm or less) are larger than the molecular diameter of the liquid ($\approx$0.25 nm for water, $\approx$0.4 nm for methanol) so that the oscillatory forces due to ordering of molecules at the interface are averaged out. This leads to a background exponential hydration (or hydrophobic) force[11,12] that is included in the simulations. We show that even though the decay lengths of the forces at the solid-liquid interface are quite small compared to the amplitudes used, the hydration/hydrophobic forces still play a large part in determining the cantilever dynamics.

## III. EXPERIMENTS

The goal for the experiments is to examine nonlinear response (amplitude and phase, including higher harmonics) of different AFM cantilevers oscillating at various liquid-solid interfaces characterized by short-range interaction forces [methanol, deionized water, and 500 mM KCl on mica; deionized water on highly oriented pyrolytic graphite (HOPG)], over a range of excitation frequencies and tip-sample $Z$ distances.

### A. Methods

Three different types of cantilevers are used in the experiments, with parameters given in Table I. The cantilevers are all rectangular and range in stiffness from 0.62 N/m to 6.6 N/m, which is typical for liquid environment imaging. Typical free (unconstrained) amplitudes are approximately 5 nm. The experiments have been replicated with multiple different cantilevers and the results are repeatable.

All of the cantilevers have been coated by Agilent with a proprietary magnetic material. This allows the use of magnetic excitation in an Agilent 5500 AFM, similar to the method described in Ref. 30. A solenoid located underneath the sample stage provides an oscillating magnetic field, which produces an oscillating torque on the cantilever. The key advantage of the magnetic excitation method is that the applied magnetic force is nearly constant over a wide range of frequencies. This allows an unobscured view of the cantilever's frequency response (as opposed to the piezo/acoustic method, which may produce many spurious resonances that are related to the piezo and not to the cantilever).

The data are collected as follows. First, the cantilever is immersed in liquid, its first eigenmode frequency determined from a thermally driven spectrum, and the magnetic excitation

TABLE I. Parameters of the cantilevers used in the experiments.

| Label | A | B | C | D[a] | E[a] |
|---|---|---|---|---|---|
| Manufacturer | Agilent | Agilent | AppNano | Agilent | Agilent |
| Model | MAC II | MAC II | ACST | MAC I | MAC II |
| Nat. freq. (kHz) | 27.4 | 32.8 | 74.4 | 19.4 | 34.3 |
| Quality factor | 3.0 | 3.5 | 5.5 | 2.3 | 5.4 |
| Stiffness (N/m) | 2.05 | 3 | 6.6 | 0.62 | 2.3 |
| Modal forcing ratio ($F_{B2}/F_{B1}$) | 5.1 | 5 | 2.5 | 1.3 | −5.2 |
| Imaging media | 500 mM KCl | Deionized water | Methanol | Deionized water | Acetone |
| Surface | Mica | HOPG | Mica | Mica | Mica |

[a]Data from cantilevers D and E can be found in the Supplemental Material (Ref. 33).

is chosen near the first eigenmode frequency. Then, the oscillating cantilever is brought closer to the surface (Fig. 1) at fixed excitation frequency until the amplitude reduces to 95% of its unconstrained value. The cantilever is stabilized at this set-point amplitude until the $Z$ drift (from thermal expansion and piezo creep) is reduced to an acceptable level (typically $<$0.3 nm/s). The normal $Z$ feedback is turned off, the $Z$ piezo voltage is adjusted to move the tip a defined distance relative to the sample, and the excitation frequency is swept up in 3–5 s. Time-series data of cantilever deflection is recorded using a National Instruments data acquisition card and processed to give mean deflection, first harmonic amplitude and phase, as well as higher harmonics. The drive frequency is returned to the resonance frequency and the $Z$ feedback is turned on. After stabilizing for one second, the $Z$ feedback is again turned off and the procedure is repeated with a different $Z$ distance from the sample.

We use three different liquids: deionized water, 500-mM KCl buffer solution (high-concentration buffer solutions are relevant to many practical imaging studies such as biological samples), and methanol (chosen because it has a lower viscosity than water). We use two different surfaces: freshly cleaved mica and HOPG.

### B. Results: Cantilever A in 500-mM KCl solution on freshly cleaved mica

Before describing the experimental results, it will be helpful to set out some notation. We shall use $A_i$ to refer to $i$th harmonic amplitude ($i = 1,2,3$, etc.) and $\phi_i$ for $i$th harmonic phase. In the modeling section, we will refer to both higher eigenmodes and higher harmonics, which are frequently confused. For example, in typical notation for quality factor $Q_2$, the subscript 2 refers to the second eigenmode, whereas when referring to amplitude $A_2$, the subscript 2 refers to the second harmonic. For clarity, a "$B$" (for "bending" following Ref. 31) will be used for a modal quantities (e.g., $Q_{B2}$ for quality factor). We will also use $A_{\text{init}}$ for the initial (free or unconstrained) amplitude.

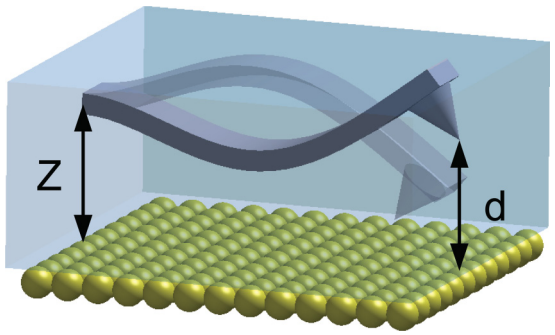


FIG. 1. (Color online) Schematic illustration of a microcantilever oscillating in liquid and approaching a solid surface.

#### 1. *Linear frequency response far from surface*

Typical results for cantilever A on mica in 500 mM KCl are shown in Fig. 2. Multiple sweeps (amplitude and phase lag of tip motion as a function of excitation frequency) are shown at progressively decreasing $Z$ distances. Before examining the nonlinear response due to tip-sample forces, we first study the linear frequency response of magnetically excited cantilevers in liquids. The sweep farthest from the sample (black dashed line) is considered first. These data are acquired far enough from the surface that the nonlinear tip-sample interactions are small enough that the response is essentially linear. Using a least-squares-curve fit, we can identify that the first natural frequency is 27 kHz [marked with a dashed line in Fig. 2(b)].

At first glance, the amplitude response [Fig. 2(a)] looks similar to that of a single degree-of-freedom oscillator. However, the phase shows an unexpected behavior. In Fig. 2(b), $\phi_1$ increases with frequency up until about 40 kHz but then reverses and decreases to nearly zero. Ordinarily, we expect the phase to asymptotically approach 180° to the right of the resonance peak. Closer inspection shows that the phase reversal is accompanied by a small antiresonance (valley) in the amplitude [Fig. 2(a)].

There is a second interesting observation about the phase signal. Most AFMs have instrumental phase offsets due to artifacts in the electronics and especially from the drive piezo. Therefore, it is common to offset the phase such that the phase at the natural frequency is 90°. The magnetic drive should be free from such artifacts, therefore we have not applied any phase offsets. As expected, the phase at zero frequency is (approximately) zero. Surprisingly though, it is apparent that the phase at the natural frequency (marked by a dashed line) is actually well below 90°.

These are two interesting observations in the cantilever response *before* it interacts with the liquid-solid interface. We have observed these phenomena while using a variety of magnetically excited cantilevers. We will describe in the

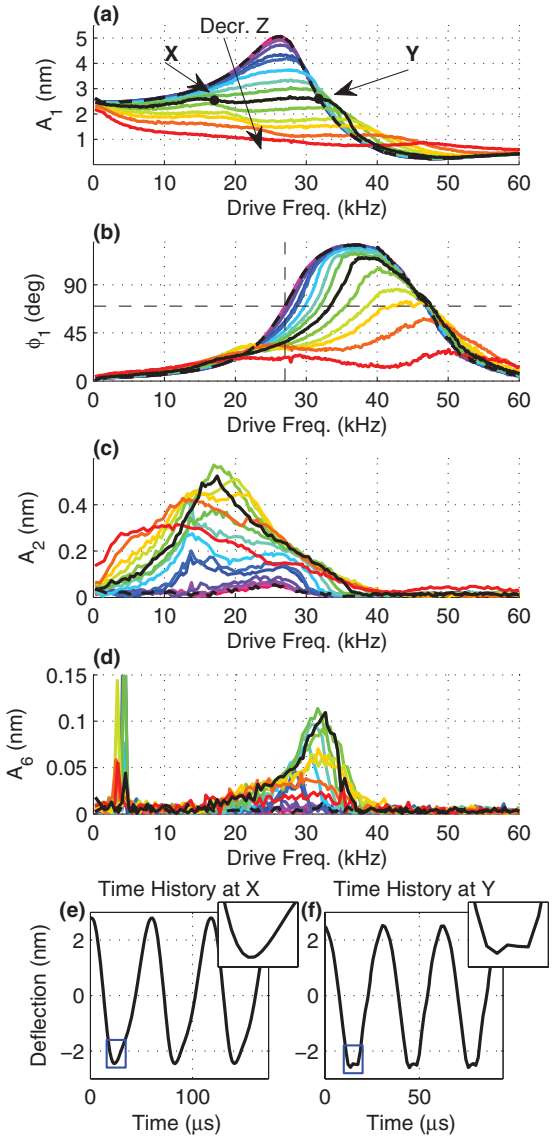


FIG. 2. (Color online) Experimental frequency sweeps for cantilever A in 500-mM KCl solution on mica. (a) $A_1$, (b) $\phi_1$, (c) $A_2$, (d) $A_6$. Interestingly, the resonance splits into two distinct peaks in $A_1$, one of which corresponds to a large $A_2$ and the other to a large $A_6$. $\phi_1$ shows an interesting reversal above resonance and surprisingly $\phi_1 \neq 90^\circ$ at the natural frequency. (e) and (f) Time histories. The signal has been comb filtered to keep only the first seven harmonics. The deflection $= 0$ point is chosen arbitrarily as there is no way to precisely determine it. The waveform shows a distinctive distortion after tapping on the sample. (e) corresponds to the black dot marked "$X$" in (a). (f) corresponds to the dot marked "$Y$". Insets: zoom-in on boxed regions.

theory section an approach that clarifies the origin of the phase behavior.

### 2. *Nonlinear response interacting with the surface*

Now, we consider the nonlinear frequency response when the cantilever is interacting with a surface. First, we will consider a single-frequency sweep at a specific intermediate distance from the surface, and then discuss how the response evolves with changing $Z$ distance. First, consider the amplitude response represented by the solid black line in Fig. 2(a). In contrast with the classical peak (black dashed lines) when not interacting with the sample, the resonance while interacting with the surface is a flat, broad peak. Closer inspection shows that there are actually two distinct peaks separated by a small valley, which is unexpected.[32] The left peak is at approximately one-half the frequency of the right peak. In other words, the amplitude response far from the sample shows a canonical response with a well-defined peak. This response, however, transforms due to forces at the solid-liquid interface into two distinct smaller peaks separated by a relatively flat plateau in-between.

Considering the phase in Fig. 2(b), it is apparent that the natural frequency while interacting with the sample has shifted to the right, as compared to the case when there is no interaction (in making this comparison, it is worth recalling that the phase lag at resonance is not 90° as discussed above). There is also a small bump in the phase just below 20 kHz, which corresponds to the same frequency as one of the two amplitude peaks due to the interaction. A well-known hallmark of nonlinear behavior is an appreciable response at frequencies other than the drive frequency (i.e., higher harmonics). In Figs. 2(c) and 2(d), the response of the second and sixth harmonics is shown (plots of other harmonics are in the Supplemental Material[33]).[19–22,24,34–41] Both of these show a small but not insignificant response. In particular, note that the $A_2$ peak occurs at the same frequency as the low-frequency peak in the $A_1$ response, and the $A_6$ peak occurs at the same frequency as the high-frequency peak in the $A_1$ response. Thus, it is clear that the two peaks have distinct causes.

Time histories of the cantilever deflection signal are shown in Figs. 2(e) and 2(f), which helps to visualize the higher harmonic components of the tip deflection waveform. The time history in Fig. 2(e) is taken at the frequency for which $A_2$ is maximum, and Fig. 2(f) is taken at the frequency for which $A_6$ is maximum. In each case, there is a distinctive distortion at the bottom of the waveform when the tip taps on the sample. The distortion is smoother in Fig. 2(e) and more pronounced in Fig. 2(f).

Now that these general features of cantilever response far from the interface and while interacting with the surface have been introduced, we can study how they evolve with $Z$ distance. From the amplitude plot in Fig. 2(a), it can be seen that the main resonance peak shifts to the right as the $Z$ distance decreases. In other words, the natural frequency increases due to the repulsive tip-sample interaction forces, as expected. This can also be seen in the phase Fig. 2(b). In air, the natural frequency first decreases due to attractive forces and then increases due to repulsive interactions.[42] In the present experiment, the attractive forces are essentially negligible and the natural frequency increases monotonically. In air, there are also jumps in the amplitude response due to the presence of multiple stable oscillation states, but those do not appear in this case. Finally, the small secondary resonances also detune (move right) as $Z$ distance decreases.

To further aid data interpretation, the same data are replotted in Fig. 3. The $Z$ displacement is along the $y$ axis and the amplitude, phase, etc., are given as a color map. From this it is easy to see that both $A_2$ [Fig. 3(c)] and $A_6$ [Fig. 3(d)]

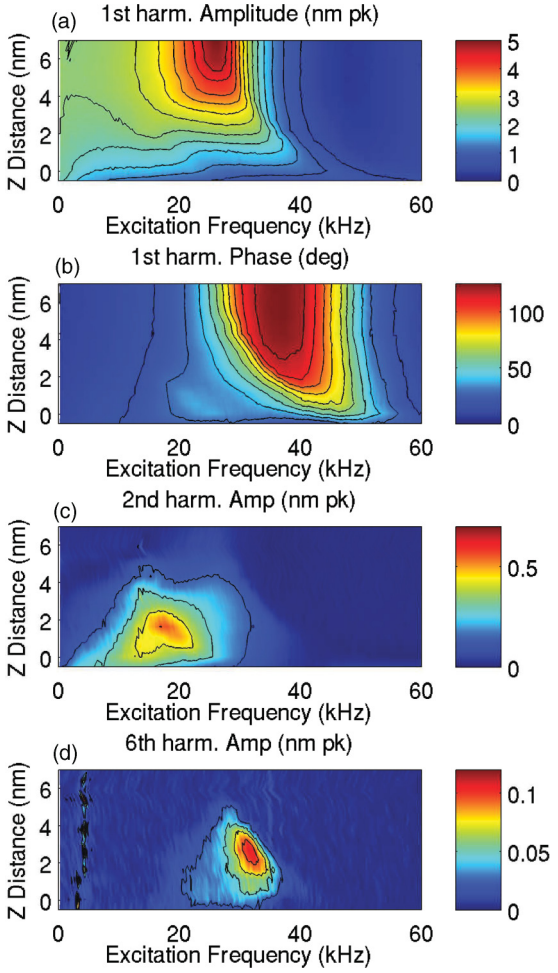


FIG. 3. (Color online) Experimental frequency sweeps for cantilever A in 500-mM KCl solution on mica. This is the same data as Fig. 2 as a contour plot. [Note: Due to contributions from the second eigenmode, the phase at the natural frequency is 80°, not 90°. See the Supplemental Material (Ref. 33) for more details]. There are 15 sweeps, each approximately 0.54 nm closer to the sample.

peak at approximately the same $Z$ distance. Some detuning of $A_2$ and $A_6$ with decreasing $Z$ distance can also be seen. The amplitude and phase response as a function of drive frequency and $Z$ distance is a dense data set with rich information about cantilever dynamics as it interacts with the surface. The frequency sweeps in Fig. 2 can be thought of as horizontal slices of the maps in Fig. 3. It is also possible to take vertical slices of the maps, which would correspond to typical dynamic approach curves. Several such slices are shown in Fig. 4. Relating the features in the frequency sweeps (horizontal slices) to the features in the approach curves (vertical slices) may serve to further illustrate the nonlinear response. In Fig. 4(b), as $Z$ is decreased, $\phi_1$ first decreases, but then increases by 5° before decreasing again. The $Z$ distance at which the phase peaks is also the same distance at which $A_2$ peaks. It is clear that the $\phi_1$ and $A_2$ behavior are related, although the cause is not immediately obvious. We will explore this further in Sec. IV.

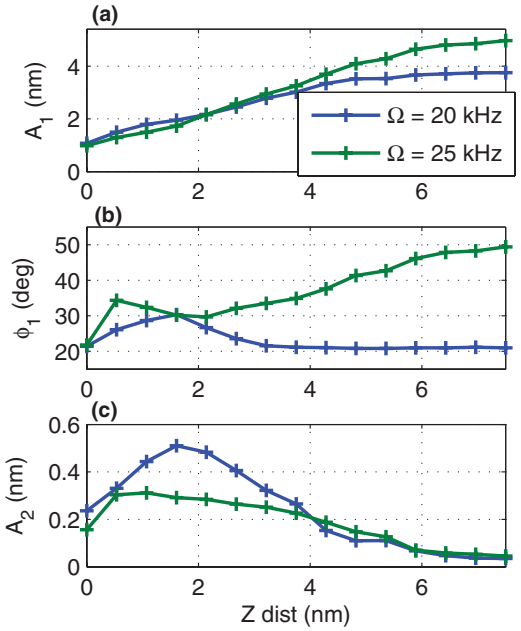


FIG. 4. (Color online) The experimental data were acquired as frequency sweeps at a series of $Z$ distances. But, we can also take vertical slices of the data set to get curves versus $Z$ for a fixed frequency (i.e., like a typical tapping mode approach curve). Here, we show $A_1$, $\phi_1$, and $A_2$ from Fig. 3 versus $Z$ for two different frequencies. The peak in $\phi_1$ and $A_2$ on the left of the graphs corresponds to the $Z$ distance at which the superharmonic resonance has detuned to the driving frequency.

### C. Results: Cantilever B in deionized water on HOPG

The previous experiments were conducted on mica, which is hydrophillic. In Fig. 5, we show an experiment on freshly cleaved HOPG, which is known to be hydrophobic. However, it is also known that due to exposure to air contaminants can cover certain terraces of HOPG,[43] which could potentially affect the hydrophobicity. In principle, we expect to see attractive hydrophobic interactions instead of the repulsive hydration interactions in the previous study on mica. Our interest is to understand if the nonlinear effects described earlier are affected by the nature of interfacial forces. The cantilever is the same model as cantilever A (i.e., same nominal parameters).

In comparison to cantilever A in 500-mM KCl solution on mica (Fig. 2), we find generally similar features of the nonlinear response, but some differences stand out. For example, the majority of the sweeps for cantilever B show only a single $A_1$ peak on the left side of the graph (and $A_2$ peaks at this same frequency). In comparison, cantilever A that showed two distinct peaks in $A_1$. This is obviously caused by some difference in the interaction forces between HOPG and mica, but it is not immediately obvious what that difference might be. In Sec. V B, we will use numeric simulations to explore the differences.

### D. Results: Cantilever C in methanol on freshly cleaved mica

Having explored how the choice of liquid-solid interface affects the nonlinear response of moderately soft cantilevers ($k_{B1} = 2$–$3$ N/m, $Q_{B1} = 3$–$4$), we now turn to understand how

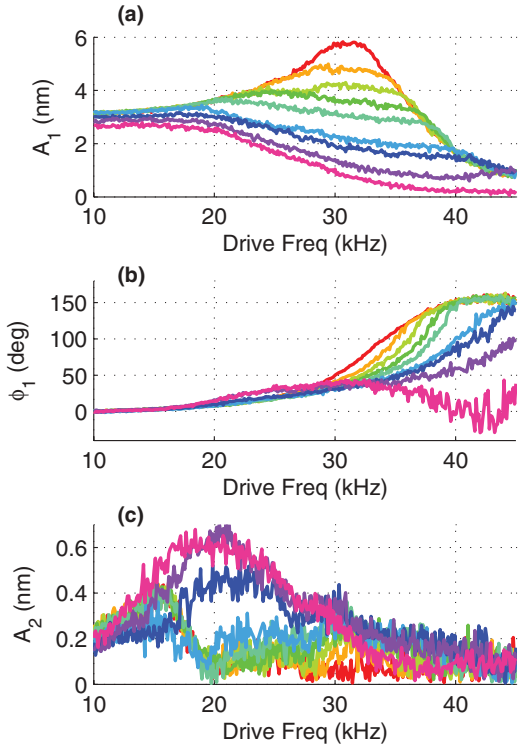


FIG. 5. (Color online) Experimental frequency sweeps for cantilever B in deionized water on HOPG. The amplitude response (a) is distinctly different than cantilever A on mica (Fig. 2). Specifically, cantilever A showed two distinct peaks in $A_1$. The majority of the sweeps for cantilever B show only one peak and it is far to the left. But based on the phase (b), the natural frequency is shifting to the right. In others, the smaller secondary resonance peak still exists, but there is no resonance peak at the natural frequency.

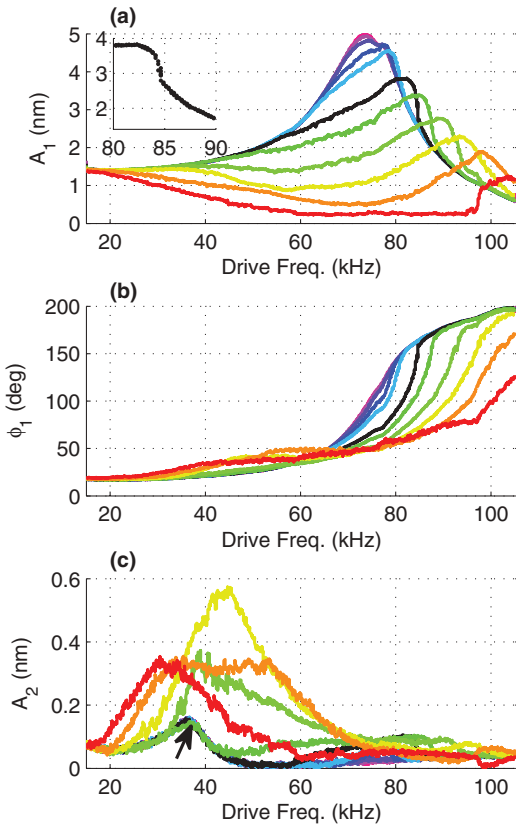


FIG. 6. (Color online) Experimental frequency sweeps for cantilever C in methanol on mica. In contrast to cantilever A, $A_2$ and the secondary peaks in $A_1$ appear to be suppressed. However, the primary resonance shows what might be a small nonlinear jump. The inset in (a) shows a zoom-in near one such jump. There are 11 sweeps, each approximately 0.54 nm closer to the sample.

the nonlinear response is affected by cantilever properties, especially higher stiffness and higher $Q$ factor. Cantilever C was chosen because it has a higher-quality factor than cantilevers A and B. To further increase $Q$, experiments with this cantilever were performed in methanol. Due to the lower viscosity, the $Q$ in methanol is about 25% higher than in water. Typical results on mica in methanol are shown in Fig. 6, and the same data plotted as contour plots can be found in the Supplemental Material.[33]

As compared to cantilever A on mica in 500 mM KCl, the second harmonic resonances in this case appear to be suppressed.[44] For cantilever A, an appreciable $A_2$ occurred for 9 out of the 15 sweeps. For cantilever C, only 4 out of 11 sweeps showed an appreciable $A_2$ (with "appreciable" being defined as $A_2 > 0.2$ nm). In addition, cantilever A showed small peaks in $A_1$ that lined up with the frequency at which $A_2$ peaked, whereas there do not appear to be any such such peaks in the amplitude for cantilever C.

The shapes of the resonance peaks are different as compared to cantilever A. Specifically, the resonance peaks for cantilever C are not broad and flat, but are strongly skewed to the right. In other words, the left side of the peak has a low slope, but the right side of the peak has a steep slope. For some of the sweeps, the slope is so steep that it appears to be a jump straight down. These features are analogous to the jumps (bifurcations) found in air/vacuum environments,[42] although less pronounced. These jumps have been previously predicted in liquids numerically.[25] We will use simulations in the next section to further investigate these features.

### E. Experimental summary

The experiments have demonstrated the nonlinear response of a variety of AFM microcantilevers on a variety of liquid-solid interfaces and have shown three distinctive features: first, even far away from the sample, the phase lag at the natural frequency is not 90°, and there is a reversal of the phase above resonance. Second, $A_1$ becomes very flat and broad when interacting with the sample and can actually show multiple distinct peaks. The lower peak is characterized by a higher $A_2$, and the higher peak by a higher $A_6$. Finally, in some cases there appear to be sudden, discontinuous jumps at the resonance peak. In the next section, numerical simulation is first used to explain these results and give insight into the physical processes at work. Then, parameter studies are given to show which parameters have the most influence on the results.

## IV. SIMULATIONS AND ANALYSIS

In this section, the VEDA (virtual environment for dynamic AFM) simulator is used to provide insight into the

experimental results. VEDA is a freely available web-based AFM simulator developed by the authors.[45–47]

### A. Cantilever modeling

The modeling starts with the Euler-Bernoulli partial differential equation for deflections of a slender, rectangular cantilever beam in a ground-fixed inertial frame, subject to a hydrodynamic damping force, a driving force, and a tip-sample interaction force

$$EI\frac{\partial^4 w(x,t)}{\partial x^4}+\rho_c A\frac{\partial^2 w(x,t)}{\partial t^2} = F_{\text{hydro}}(w)+F_{\text{drive}}(x,t)+F_{ts}[w(L,t)+Z]\delta(x-L), \tag{1}$$

where $E$, $I$, $\rho_c$, $A$, $w$, $x$, $t$, $F_{\text{hydro}}$, $F_{ts}$, $F_{\text{drive}}$, and $\delta$ are the cantilever Young's modulus, area moment, density, cross-sectional area, deflection, axial coordinate, time, hydrodynamic force, tip-sample interaction force, driving (excitation force), and the Dirac delta function, respectively. The hydrodynamic forces are converted into an effective modal viscosity and added mass,[35,48] and then the equation is discretized in the basis of cantilever eigenmodes using Galerkin's method following Ref. 49. The method is to write $w$ as $w(x,t)=\sum_{i=1}^{\infty} q_i(t)\psi_i(x)$ where $\psi_i(x)$ is the $i$th eigenmode shape and $q_i(t)$ is referred to as a modal coordinate.[50] An approximation is made by keeping only the first $N$ eigenmodes. We take $N=3$ in this work.[51] This reduces the original equation to a set of $N$ ordinary differential equations:

$$\frac{\ddot{q}_i}{\omega_{Bi}^2}+\frac{\dot{q}_i}{\omega_{Bi}Q_{Bi}}+q_i=\frac{F_{ts}(d)}{k_{Bi}}+\frac{F_{Bi}\cos\Omega_d t}{k_{Bi}}, \quad i=1,\ldots,N \tag{2}$$

where $q_i(t)$, $\omega_{Bi}$, $Q_{Bi}$, $k_{Bi}$, and $F_{Bi}$ are the tip deflection, natural frequency (rad/s), quality factor, equivalent stiffness, and driving force of the $i$th eigenmode, respectively, $d=Z+\sum_{i=1}^{N} q_i$ is the tip-sample gap, where $Z$ is the cantilever-sample separation, and $\Omega_d$ is the driving frequency (rad/s). See Fig. 1 for an illustration of $Z$ and $d$. Again, the "$B$" in the subscript emphasizes that the subscript refers to a bending eigenmode (as opposed to a harmonic). In our experiments, $k_{B1}$ is calibrated in air using the method of Ref. 52. $k_{Bi}$ for $i>1$ is calculated using the result of Ref. 35 with the details given in the Supplemental Material.[33]

In air or vacuum, the modeling of the excitation force is unimportant as all methods give essentially the same result. In liquids, the different methods give dramatically different results.[39] Magnetic excitation is used in the present experiments because it gives good results in liquids, therefore we focus on it here. Discussion on the dynamics of other methods are given in Refs. 39, 40, and 53, as well as in the Supplemental Material.[33]

The cantilever is coated with a magnetic material magnetized along the length of the cantilever and an oscillating external magnetic field is applied. The exact nature of magnetic forcing on the cantilever is an ongoing research topic. In principle, if the magnetic field is uniform and perpendicular to the axis of magnetization, then the modal force on each eigenmode is the same ($F_{B1}=F_{B2}=F_{B3}$, etc.).[54] However, in practice, the magnetic field may be far from uniform, so the ratio $F_{B2}/F_{B1}$ must be determined empirically by fitting $F_{B2}/F_{B1}$ such that the measured amplitude and phase response match with the model predictions [Eq. (2) without interaction forces]. Details on the fitting procedure are given in the Supplemental Material. Depending on the location of the cantilever relative to the solenoid, $F_{B2}/F_{B1}$ has been observed to take values anywhere between $-5$ and 25.

To model the optical beam deflection method, observed deflection is reported as $\tilde{u}=\sum_{i=1}^{N}(\chi_{Bi}/\chi_{B1})q_i$ where $\chi_{Bi}$ is the slope at the end of the $i$th eigenmode. In our experiments, the photodiode volts-to-nanometers conversion has been calibrated for the first eigenmode using the method of Ref. 55. $\chi_{Bi}$ for $i>1$ is difficult to calibrate experimentally. We calculate it according to the results of Ref. 35, with the details given in the Supplemental Material.[33]

### B. Tip-sample interaction force models

Based on the experimental conditions described, we propose a tip-sample interaction force that is composed of two parts and is a reasonable approximation for the different liquid-solid interfaces considered in this work. The first part of the force is the noncontact force. For the experimental conditions in this work and for other practical experimental conditions, the attractive van der Waals force is small. The electrical double-layer force is effectively screened in high-concentration ionic media, and in the case of deionized water (as in the present experiments), the gradient of this force is negligible over length scales of the tip oscillation amplitude. Oscillatory forces are neglected because the cantilever amplitudes are large enough that the oscillations average out. Therefore, the only noncontact forces are the short-range hydration/hydrophobic forces.

The hydration force is so named because it may be linked to the energy required to remove hydrated water molecules from the surface. A typical model is exponential decay[11,12,29]

$$F_{ts,\text{hyd}}(d)=\begin{cases}2\pi R^2 p_h \exp\left(-\frac{d}{\lambda}\right), & d>0\\ 2\pi R^2 p_h, & d\leqslant 0\end{cases} \tag{3}$$

where $R$ is the tip radius, $\lambda$ is a decay length, and $p_h$ is an empirically determined scaling. The same model is used for hydrophobic forces, except the sign of $p_h$ is changed.

In addition to conservative forces, it has been recognized that there are also dissipative (nonconservative) components to the hydration/hydrophibic forces. There is still debate as to the exact form of these forces.[56,57] Several works[29,58,59] have considered how well this damping is modeled by continuum Reynold's squeeze film damping $F=-6\pi\eta_{\text{eff}}R_{\text{tip}}^2\dot{d}/d$ where $\eta_{\text{eff}}$ is an "effective" viscosity. These authors have noted that in order to account for the experimentally observed energy dissipation, an effective viscosity several orders of magnitude larger than the bulk value is required. Further, the required effective viscosity $\eta_{\text{eff}}$ is not constant, but must be a function of tip-sample gap[59] $d$. Finally, the model clearly breaks down as $d\to 0$.

Therefore, rather than try to find an "effective" viscosity profile that forces the continuum model to match the observed experimental data, we look for a simpler model that will directly match the experimental data. Reference 29 made

the observation that the damping coefficient appeared to be proportional to the conservative portion of the force. Therefore, analogous to (3), we propose a viscous drag where the damping coefficient decays exponentially away from the wall. Letting $c$ be a scaling (kg/s), the force is given by

$$F_{ts,\mathrm{diss}}(d,\dot{d}) = \begin{cases} -ce^{-d/\lambda}\dot{d}, & d > 0 \\ -c\dot{d}, & d \leqslant 0. \end{cases} \tag{4}$$

The damping coefficient is assumed to saturate to a constant value once the tip and sample contact (similar to the way that the attractive forces in the DMT model saturate at contact). For the present experiments, the samples are stiff, so the indentations are small (<1 Å). Therefore, the exact behavior of the hydration force for $d < 0$ does not have a large effect on the cantilever motion. For softer materials such as lipid bilayers,[60] more sophisticated modeling may be necessary.

The second part of the force is a contact force. The classical Hertz contact theory[61] for the force between a sphere and a flat plane is given by

$$F_{ts,\mathrm{Hertz}}(d) = \begin{cases} 0, & d > 0 \\ \frac{4}{3}E^*\sqrt{R}d^{3/2}, & d \leqslant 0 \end{cases} \tag{5}$$

where $E^*$ is the reduced elasticity $E^* = [(1-\nu_{\mathrm{tip}}^2)/E_{\mathrm{tip}} + (1-\nu_{\mathrm{sample}}^2)/E_{\mathrm{sample}}]^{-1}$ and $\nu$ and $E$ are Poisson's ratio and Young's modulus of the tip and the sample.

The total force model used in this work is thus

$$F_{ts}(d) = F_{ts,\mathrm{hyd}}(d) + F_{ts,\mathrm{diss}}(d,\dot{d}) + F_{ts,\mathrm{Hertz}}(d). \tag{6}$$

An example plot of a typical force curve is shown in Fig. 7. Importantly, the hydration forces have a relatively smooth exponential decay, and the transition to Hertz[62] contact at $d = 0$ is comparatively abrupt. The area enclosed by the curve represents the nonconservative energy dissipation.

It is assumed that the sample does not deform at all until the tip contacts the sample. In reality, the hydration forces and contact forces are like springs in series. Thus, the sample can deform due to the hydration forces. The samples considered here are stiff enough that any such deformation would be negligibly small. For softer samples,[60] more sophisticated modeling may be necessary.

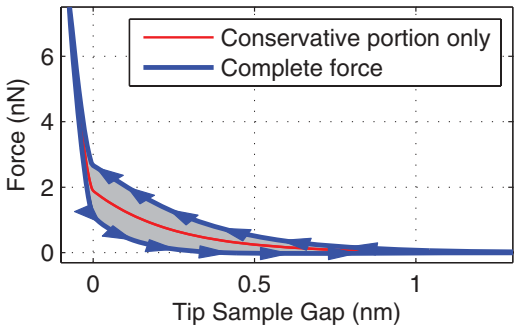


FIG. 7. (Color online) Example tip-sample interaction profile used in the simulations. An exponentially decaying hydration force, which has both a conservative and a nonconservative component, extends from gap = 0 to the right and a Hertz contact force extends from gap = 0 to the left. The plot shown is for $\Omega_d = 10$ kHz, $A = 3.1$ nm, and $Z = 1.45$ nm.

TABLE II. Simulation parameters.

| | |
|---|---|
| Natural freq. (kHz) | $\omega_{B1} = 27.6$, $\omega_{B2} = 179$, $\omega_{B3} = 484$ |
| Stiffnesses (N/m) | $k_{B1} = 2.1$, $k_{B2} = 63.6$, $k_{B3} = 447$ |
| Quality factors | $Q_{B1} = 3$, $Q_{B2} = 8.3$, $Q_{B3} = 12$ |
| Unconstrained ampl. | $A_{\mathrm{init}} = 5$ nm |
| Sweep time | 2 s |
| Tip radius | 10 nm |
| Sample Young's modulus | 60 GPa |
| Hydration decay length | $\lambda = 0.25$ nm |
| Hydration force scaling | $p_h = 3 \times 10^6$, $c = 2.6 \times 10^{-5}$ (kg/s) |

The simulation parameters are given in Table II.

### C. Linear frequency response far from sample

We are now in a position to explain the curious features in the phase noted in Sec. IV C. In Figs. 8(a) and 8(b), an experimental frequency sweep far from the sample is compared with simulated data. We have plotted not only the simulated photodiode signal, but also the responses of the first and second eigenmodes separately. It is clear that the response of the second eigenmode is (relatively) large. In other words, the quality factors are so low that the second eigenmode can be excited appreciably even when the excitation frequency is close to the first natural frequency. Because the first and second eigenmode responses are out of phase with each other, they partially cancel, resulting in the observed antiresonance in the amplitude and the reversal in phase. This also explains

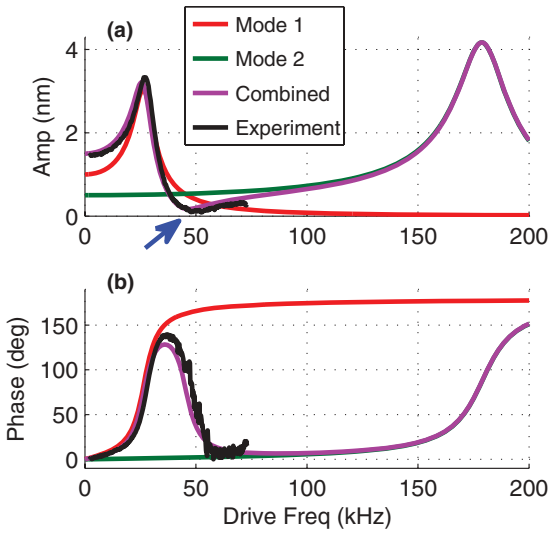


FIG. 8. (Color online) Experimental frequency sweeps for cantilever A in 500-mM KCl solution far (>2 $\mu$m) away from any surface compared with simulated frequency sweeps showing the response of each eigenmode individually and combined. Due to the low-quality factors, the second eigenmode can be excited appreciably off resonance. Near 50 kHz, the amplitude response of the second eigenmode partially cancels out the first eigenmode, resulting in an antiresonance (marked with an arrow).

why the phase lag at the first natural frequency was not 90°. The phase of the first eigenmode by itself is 90°, but what we are observing with the photodiode is the sum of multiple eigenmode responses.

To some degree, this effect will be present in all magnetically driven AFMs. The important consideration is how close the antiresonance is to the fundamental resonance. In some cases, it will be far away and thus can be neglected. Two reasons that the resonance and antiresonance are so close in the present case are the picket-shaped end of the MAC II cantilever and the nonuniform magnetic field from the solenoid, as explained in the Supplemental Material.[33] It should be noted that even linear (i.e., small amplitude) measurements can potentially be affected by this. Standard force spectroscopy formulas that consider only the response of a single eigenmode (e.g., Ref. 63) could thus be significantly in error. More details are shown in the Supplemental Material.[33]

Finally, we note that while the acoustic excitation method has been criticized for piezo resonances and large base motion, which greatly impede quantitative dynamic AFM,[28,39,40,64] this result shows that the magnetic method is not without its own subtleties. The key point is that any quantitative analysis for low-quality factors ($Q < 10$) requires careful attention to the mechanics of the excitation.

### D. Nonlinear frequency response while interacting with the liquid-solid interface

In this section, we attempt to reproduce the results of cantilever A on mica in water in Sec. III B in order to verify the model. The simulation parameters are given in Table II. The hydration force decay length of 0.25 nm is approximately the diameter of a water molecule, as determined experimentally by Ref. 29. The hydration force scaling parameters $p_h$ and $c$ were determined by matching experimental approach curves to simulations and are similar to the values used in Ref. 46. A positive value of $p_h$ corresponds to a repulsive hydration force. Although the hydration damping model is different than previous works, the effective damping coefficient is on the same order as previous work.[29,59] Discussion on the parameters for HOPG will be given in a later section.

Figure 9 shows the results, and more plots are available in the Supplemental Material.[33] The results compare favorably to the experiments. All of the significant features of the experiments discussed in Sec. III are present in the simulation. The only significant discrepancy between the simulation and the experiment is the amplitude of the higher harmonics. The general shape and trend of $A_6$ in Fig. 9(d) matches that in Fig. 2(d), however, the simulated amplitude is twice as high as the experiment. There are several possible explanations.

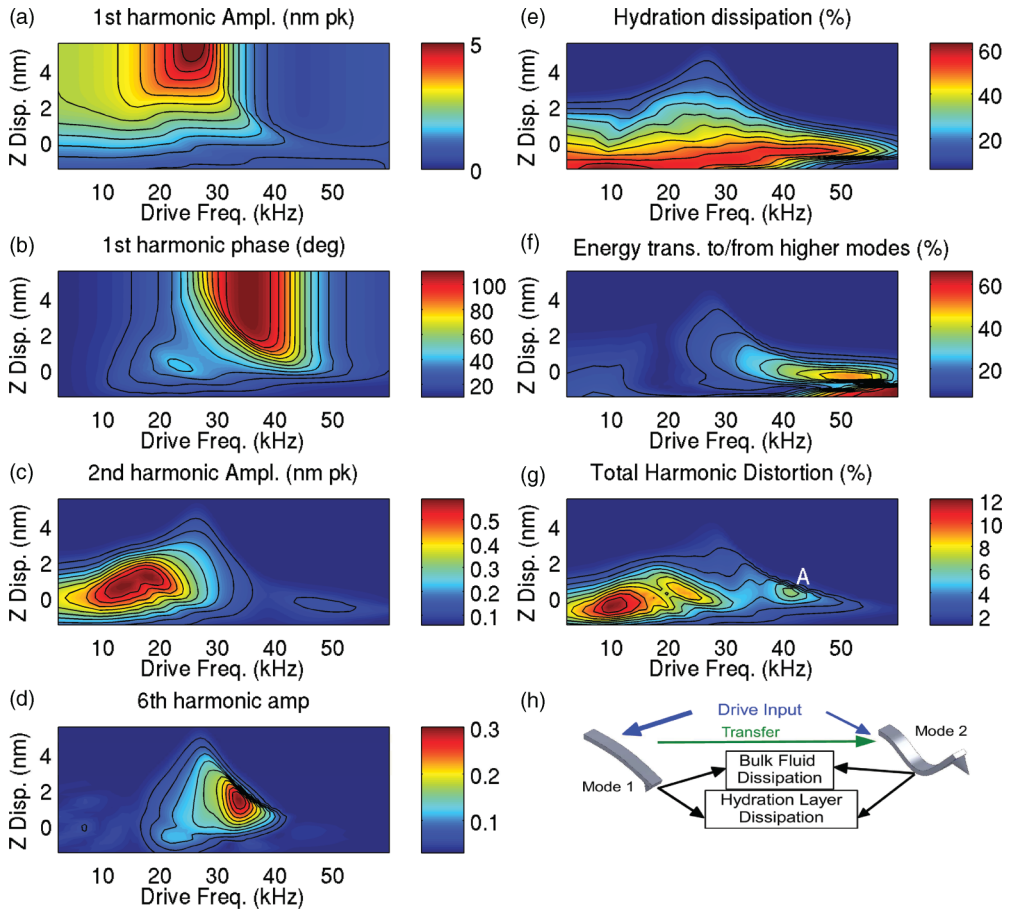


FIG. 9. (Color online) Simulated frequency sweeps plotted as a map with $Z$ distance and excitation frequency along the axes and the value given by the color. (a)–(d) are compared to the experimental observables in Fig. 3 (cantilever A on mica in 500 mM KCl), while (e)–(g) represent analytically computed quantities that may not be directly observable in the experiment. (h) Schematic of energy flow (third mode omitted for clarity).

First, our model parameters might be somewhat in error. The most sensitive parameters are the quality factor and natural frequency of the second eigenmode. A 1% decrease in $Q_{B2}$ leads to a 1% decrease in $A_6$ and a 1% decrease in $\omega_{B2}$ leads to a 0.6% decrease in $A_6$.

Second, the form of models themselves could be incorrect. For example, the bulk hydrodynamic damping is being represented by linear viscous damping, when the frequency-dependent hydrodynamic function would be more accurate. Similarly, the nonconservative tip-sample interaction model is assumed to be frequency independent, while in reality there may be some frequency dependence. The error incurred in the approximation of the bulk damping is expected to be small (see Supplemental Material[33]). However, it is more difficult to quantify the magnitude of potential modeling errors in the tip-sample interaction. Given the high sensitivity of the response to the higher eigenmode parameters, and the fact that these parameters are difficult to calibrate, we believe the most likely source of the discrepancy is the calibration of these parameters. Nonetheless, the qualitative features of the theoretical predictions are remarkably close to those observed in experiments.

### E. Discussion

Now that we have shown that the model matches the experimental results, we can begin to discuss the results in terms of nonlinear dynamics and use the model to explain the observed features. The experimental result in Sec. III B showed that the resonance split into two separate peaks. Each of these will be discussed separately. Following nonlinear dynamics convention, the right peak (the one associated with the natural frequency) will be referred to as the *primary resonance*, and it is discussed first.

In Fig. 2, we noted that the primary resonance corresponded to a peak in $A_6$. We choose to plot the sixth harmonic because it was the harmonic with largest amplitude response. $A_5$ also shows a large response at the primary resonance. The response of other higher harmonics are lower (see Supplemental Material[33]). Why should the fifth and sixth harmonics be the highest? Based on the model, it is obvious that those are the higher harmonics that lie in the center of the bandwidth of the second eigenmode. The higher harmonics represent the second eigenmode being momentarily excited and then ringing down, as in Ref. 14. In other words, when the tip taps on the surface, energy is transferred from the driving frequency into higher frequencies and higher eigenmodes. Some implications of this energy transfer are discussed in Refs. 19–21.

In the context of nonlinear dynamics, two types of nonlinear forces can be distinguished, which are referred to as hardening and softening.[65] In a hardening nonlinearity, the effective stiffness increases as the amplitude of oscillation increases. Examination of the tip-sample interaction forces [Eqs. (3) and (5)] shows that both are hardening nonlinearities. As the cantilever oscillation increases, the tip will indent the sample more and the effective sample stiffness increases. Therefore, we expect that the primary resonance should show characteristics that are associated with hardening nonlinearities. One such characteristic is that the primary resonance peak should not be symmetric, but be skewed toward the right. This is exactly the behavior observed in the experiment, most notably in Fig. 6. A strong hardening nonlinearity can also cause the coexistence of multiple stable oscillation states (e.g., the attractive and repulsive regimes in tapping mode in air/vacuum). The simulations in Fig. 9 did not show any such feature, however, Fig. 6 suggests that they may be possible in liquids for some combinations of parameters. We will return to the subject in Sec. V C.

Now, we consider the secondary resonance peaks. Recall that there was a peak in $A_2$ when the cantilever was excited at one-half the natural frequency. In other words, the cantilever is being excited at one-half its natural frequency and it responds at the natural frequency. Because there is a response at a higher frequency than the excitation frequency, we refer to this situation as a *superharmonic resonance*.[66] The origin of the superharmonic resonance is the nonlinear tip-sample interaction. Its existence can be shown analytically through perturbation analysis.[65] Such analysis shows that superharmonic resonances are possible when the excitation frequency is an integer fraction of the natural frequency (one-half, one-third, one-fourth, etc.) and will have a larger amplitude when the nonlinearity is "stronger." We will discuss various parameters that affect the strength of the nonlinearity (e.g., cantilever stiffness), as well as address the question of why these superharmonic resonances do not occur in air in Sec. V.

We are now in a position to explain the peak in phase in the approach curves of Fig. 4. As the cantilever approaches the surface, the superharmonic resonance detunes (moves right) due to the repulsive tip-sample interaction forces. The peak in $\phi_1$ (and $A_2$) is the point at which the superharmonic resonance has detuned to near the drive frequency. A similar peak in phase versus $Z$ distance plots was found by Ref. 13. In that work, peaks in phase were attributed to a transition to a multiple impact regime (i.e., the tip taps on the sample twice during one drive cycle). This peak, however, is caused by the superharmonic resonance and does not represent a multiple impact regime.

We can also use the theoretical model to examine quantities that are not directly observable in the simulation in order to provide physical insight to the system. For example, it is useful to understand the flow of energy in the system [illustrated schematically in Fig. 9(h)]. Because the simulated sample surface is elastic (conservative), all of the energy input by the drive is eventually dissipated into either the bulk fluid media, or into the hydration layers just above the sample. The percentage of the dissipation that is due to the hydration layers is plotted in Fig. 9(e). Although there is some variation of dissipation with frequency, the strongest effect is simply the $Z$ distance. When the cantilever is closer to the surface, it spends more time in the vicinity of the hydration layers and thus dissipates more energy into them. The exception is the bottom right of the plot: this is where the cantilever is in permanent contact with the sample and is thus not traversing the hydration layers.

In Fig. 9(f), the energy transferred by the tip-sample interaction into (or out of) the second and third eigenmodes is plotted. This quantity is large along the primary resonance, but close to zero near the superharmonic resonance. In other words, at the superharmonic resonance, energy is transferred to higher frequencies (i.e., second and third harmonic), but the energy stays in the first eigenmode. At the primary

resonance, energy is transferred both to higher frequencies and higher eigenmodes.[19,67] Note from the energy flow diagram [Fig. 9(h)] that some of the energy that is transferred from the first mode to higher modes is eventually dissipated into the hydration layers, so Figs. 9(e) and 9(f) may add up to more than 100%. Finally, in Fig. 9(g), total harmonic distortion is plotted [THD $= (\sum_{i=2}^{\infty} A_i^2)/A_1^2$]. This represents the percentage of power that is being transferred to higher harmonics and is good indication of the total amount of nonlinearity present in the system. The largest amount of THD is on the left side of the graph, in the areas where superharmonic resonances are present. Comparatively, the THD along the backbone of the primary resonance has a much smaller peak at the point labeled "A."

The findings in this section can be summarized as follows: Both the primary and secondary resonances involve significant energy transfer to higher frequencies. For the primary resonance, a large portion of this energy is going to higher eigenmodes. On the other hand, for the secondary resonances (which are at integer fractions of the primary resonance frequency), the energy stays mainly within the first eigenmode. At every frequency, there is a large energy dissipation into the hydration layers, and this increases as the tip approaches closer to the surface.

## V. PARAMETER STUDIES

In the previous section, we simulated the results for cantilever A on mica in buffer solution and then used the model to explain some of the salient features. In this section, we use simulations to study the effects of various parameters to provide further insight into the nonlinear dynamics.

### A. HYDRATION FORCES

As seen in Fig. 7, the hydration forces appear to be relatively small and smooth compared to the Hertz contact forces. How much, then, do the hydration forces contribute to the type of nonlinear effects observed in liquids? Figures 10(a) and 10(b) show a set of simulated frequency sweeps in which the hydration forces are removed (Hertz only). The simulation without hydration forces shows greatly enhanced superharmonic resonances. In fact, two, three, or four distinct superharmonic resonances can be seen on various sweeps. The simulation with the hydration forces shows a reduced, smoothed superharmonic. Further, the primary resonance peak is highly skewed to the right, with large sudden jumps. This is indicative of a strong stiffening nonlinearity. From this simulation, it is clear that the presence of the hydration force in the tip-sample interaction model is essential to reproducing the experimental results. This indicates that the hydration forces play a large role in determining the cantilever dynamics at the interface.

Why do the hydration forces have such a large impact on the dynamics? For one, they add an additional damping/energy dissipation to the system. We expect nonlinear behaviors to be suppressed by damping. Further, the hydration forces smooth out the abrupt transition from noncontact to Hertz contact. To illustrate this, we show the time history of tip-sample gap and tip-sample force from two simulations in Figs. 10(c) and 10(d). One simulation includes hydration forces and the other is Hertz contact only. The time history of tip-sample force is clearly quite different. For the Hertz contact model, the force is a short, impulsive spike, whereas for the hydration forces model, the force is much lower and broader. In both cases, higher harmonics of the force excite higher harmonics of the cantilever deflection when the tip taps on the sample.[14] However, the hydration forces smooth out the force such that the higher harmonics of the force are smaller.[68]

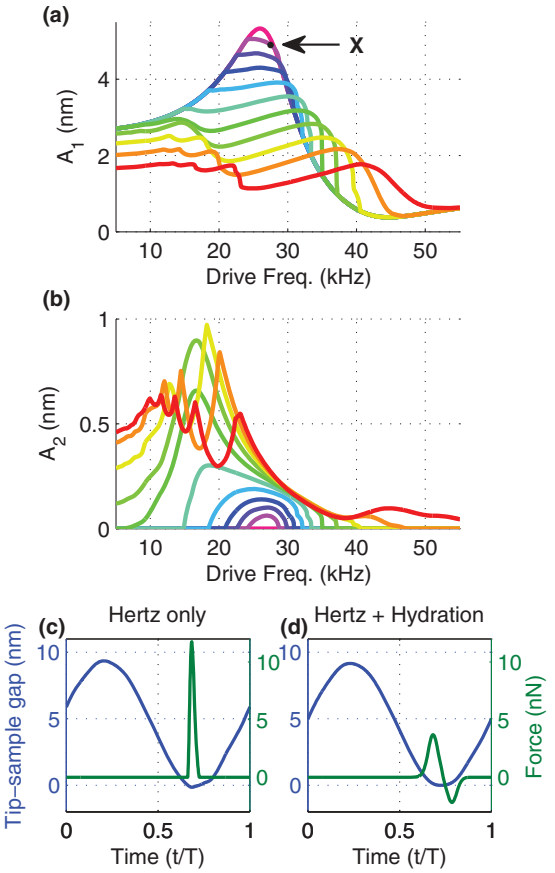


FIG. 10. (Color online) (a), (b) Simulations for the parameters given in Table II (cantilever A on mica) except hydration forces are zero (i.e., the only force is Hertz contact). As compared to the experiments (and the simulations with hydration forces), these simulations show significantly more pronounced nonlinear features. Some of the sweeps show three or four distinct superharmonic resonance peaks, and the primary resonance shows large jumps. As these features are not seen in the experiments, we can infer that the effect of the hydration forces is to smooth out the nonlinear forces and reduce the nonlinear behavior. (c) and (d) Time histories at the point marked $X$. (c) shows a model without hydration forces (Hertz only), while (d) shows the model with hydration forces. For the Hertz model, the interaction is a short impulsive spike. The hydration forces, however, smooth out the interaction to a smoother broader pulse.

### B. Effect of different surfaces

In the experiments, cantilever A on mica showed a different response than cantilever B on HOPG. In this section, we consider what differences in surface forces might be responsible for this behavior. Mica is hydrophillic, whereas

HOPG is hydrophobic. In general, the surface forces between hydrophobic surfaces are expected to be attractive.[11] Further, the hydration forces of water on mica were found to have a decay length approximately equal to the molecular diameter, but this is not necessarily always the case. Decay lengths of up to 1–2 nm have been reported on hydrophobic surfaces.[12] Therefore, we simulated frequency sweeps with the same parameters as in Table II, except the decay length is doubled ($\lambda = 0.5$ nm) and the conservative force [Eq. (3)] is changed to be attractive and reduced in magnitude by one-third. Note the scaling on the nonconservative force [Eq. (4)] is the same, only the decay length is changed. These parameters were determined based on approach curves.

The results in Fig. 11 are consistent with the experimental observations. Specifically, there is only a single peak in amplitude at the superharmonic resonance and then $A_1$ decreases monotonically to the right. Note that the natural frequency is shifting to the right due to the repulsive forces from the Hertz contact. However, the stronger damping force [Eq. (4)] is reducing the cantilever amplitude so much that there is no distinct peak at resonance. The fact that the scaling of the nonconservative forces appear to be similar on both mica and HOPG appears to be at odds with other works that studied the solvation forces above hydrophobic surfaces,[41,69,70] which found the effective viscosity of water above a hydrophobic surface to be significantly lower than that of water above a hydrophillic surface. For example, Ref. 41 found the effective damping coefficient above HOPG to be 41% of the value above mica. In our simulations, reducing the damping coefficient that much gives a result that is not consistent with our experiments (see Supplemental Material[33]). None of these works considered tapping-mode AFM, however, so there may be some salient difference between their techniques and ours. Alternatively, it is possible that there was some contamination on our sample which affected the result. Previous authors have argued for contamination layers as an explanation for other unexpected experimental results on HOPG.[71]

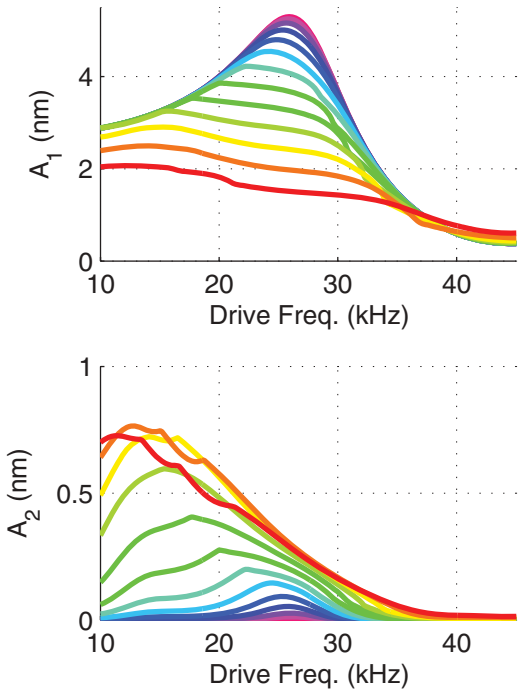


FIG. 11. (Color online) Simulated frequency sweeps using the parameters in Table II, except the decay lengths are doubled ($\lambda = 0.5$) and the scaling is changed to weak attraction ($p_h = -1e6$) in order to model the hydrophobic forces on HOPG (in deionized water). The simulation qualitatively matches the experiments HOPG (Fig. 5) in that there is only a single peak in the amplitude at the superharmonic and no peak at the primary resonance.

### C. Effect of quality factor on the nonlinear response

In the experiments, the effects of quality factor and stiffness are difficult to separate. This is because quality factor is not an independent quantity but a nondimensional ratio $Q_{Bi} = \sqrt{k_{Bi} m_{Bi}}/c_{Bi}$, where $c_{Bi}$ is the hydrodynamic damping coefficient of the $i$th eigenmode. Further, $k_{Bi}$, $m_{Bi}$, and $c_{Bi}$ are themselves functions of the beam and fluid parameters. Therefore, it is often not possible in experiments to change one parameter independently of the others.[72] For example, cantilevers A and C differed in both quality factor and stiffness. Which factor was responsible for the different nonlinear response, the modal stiffness or the $Q$ factor or a combination of both? Or was it some other parameter such as tip radius? Simulations are useful in answering these questions because exactly one parameter can be changed at a time. In this section, we study the effect of quality factor by itself, and then in Sec. V D we examine the effect of stiffness by itself.

#### 1. Superharmonic resonances

In Fig. 12, a series of simulations is shown for varying quality factor (keeping cantilever stiffness and all other parameters constant). As $Q$ is increased, the superharmonic resonances are suppressed as evidenced by the decreased $A_2$ as well as the reduced peaks in $A_1$. For the superharmonic resonance to occur, the tip generally needs to be in intermittent (Hertz) contact with the sample when the drive frequency is approximately half the effective natural frequency. The hydration forces are relatively smooth and do not provide sufficient nonlinearity to generate a superharmonic resonance. For a low-quality factor, the broad resonance peak means that the tip is in intermittent contact for a wide range of frequencies and $Z$ values. For higher-quality factors, the narrow resonance peak means that the tip is in intermittent contact only for drive frequencies near the resonant frequency or for very low-$Z$ values. Thus, for high-quality factors, the superharmonic resonance can only occur when the $Z$ distance is very low. This explains why the superharmonic resonances are not observed in air/vacuum: the cantilever would need to be driven far off resonance while positioned only a few picometers above the surface.

#### 2. Primary resonance

Recalling Fig. 9(g), the total harmonic distortion along the primary resonance peaked at an intermediate $Z$ value (point "A"). Thus, in inspecting Fig. 12, we see that for high-$Z$ values, the primary resonance is linear for all the different quality factors (because there is no tip-sample interaction force).

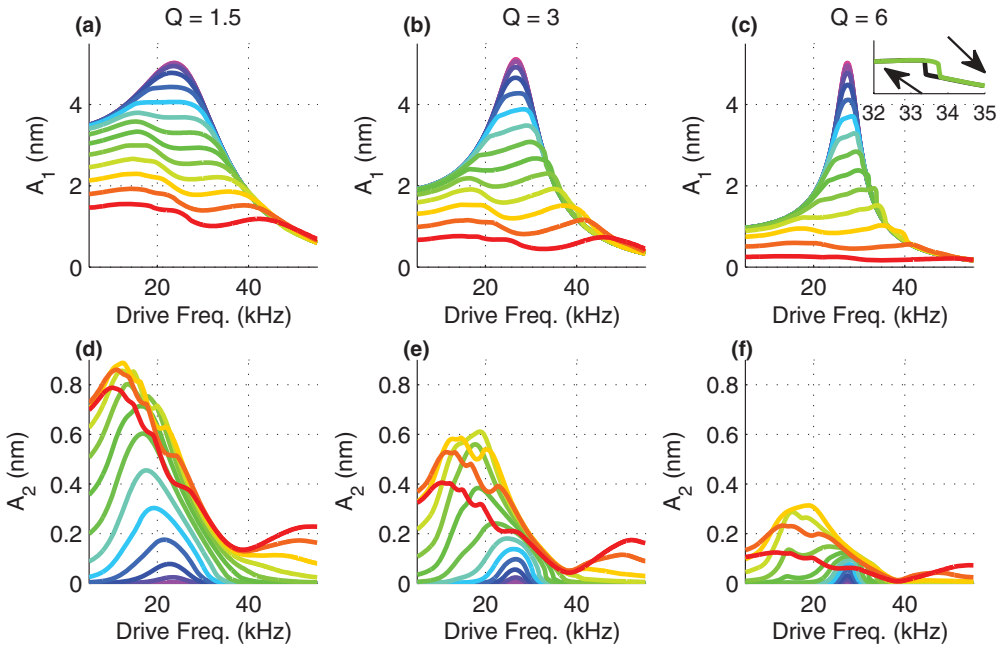


FIG. 12. (Color online) The effect of quality factor on the nonlinear response. The parameters are the same as in Table II (cantilever A on mica) except $F_{B2}/F_{B1} = 1$ and the first quality factor $Q_{B1}$ is varied (the ratios $Q_{B2}/Q_{B1}$ and $Q_{B3}/Q_{B1}$ are kept constant). The inset in (c) compares a sweep up and a sweep down at $Z = 1.5$ nm.

Similarly, for low-$Z$ values (as the cantilever approaches permanent contact), the primary resonances for all $Q$ values essentially resemble a linear peak that has been shifted to the right. The most pronounced effect of changing quality factor is thus at the intermediate $Z$ values.

As $Q$ increases, the primary resonance peak starts to resemble that of a classical stiffening nonlinear resonance peak. That is, the resonance peak is not symmetric, but rather skewed to the right. There is a long ramp up to the peak value and then a much more abrupt ramp down. In fact, for sufficiently high-quality factors, the resonance peak develops a sudden discontinuous jump straight down [inset in Fig. 12(c)], exactly as seen in the experiments in Sec. III C. This resembles the jumps found in air/vacuum environments.[42] A hallmark of this type of nonlinear effect is that there is a hysteresis in the frequency of the jump when sweeping up versus sweeping down in frequency, as shown in the inset. In other words, there are multiple stable oscillation states. Therefore, we can conclude that nonlinear effects are relevant in liquids regardless of quality factor. For low-quality-factor cantilevers, the dominant nonlinear effect is superharmonic resonances. For high-quality-factor cantilevers, the dominant nonlinear effect is the stiffening nonlinearity near the primary resonance.

### D. Effect of cantilever stiffness on the nonlinear response

In Fig. 13, the effects of cantilever stiffness are considered (keeping quality factor constant). Considering the first three cases [Figs. 13(a)–13(c)], the primary resonance, which is barely distinguishable from the superharmonic resonance for the $k_{B1} = 0.5$ N/m case, becomes a pronounced peak that is skewed to the right for $k_{B1} = 8.2$ N/m. In fact, jump phenomena develop for one $Z$ distance. Second, the superharmonic resonance becomes more pronounced as stiffness is increased from 0.5 to 8.2 N/m. In fact, multiple distinct superharmonic peaks develop in $A_1$. Both observations lead to the conclusion that increasing the cantilever stiffness is increasing the strength of the nonlinear response.

But, this is exactly opposite the conclusion of previous studies,[19,20,22] which suggested that increasing cantilever stiffness leads to less nonlinear effects. The resolution of this apparent contradiction is that the previous studies considered only Hertz contact forces and did not account for the effects of hydration forces. When both forces are included in the model (and again keeping quality factor constant $Q_{B1} = 3$), we can distinguish two regimes:

(1) For cantilevers with low to medium stiffness ($k_{B1} < \sim 20$ N/m), the cantilever is detuned by the both the hydration forces and the Hertz contact forces. Increasing the cantilever stiffness in this regime reduces the relative contribution of the hydration forces and increases the relative contribution of the Hertz contact forces. The Hertz contact forces are a stronger nonlinearity than the hydration forces, therefore, increasing the stiffness in this regime increases the nonlinearity of the response.

(2) For a very stiff cantilever ($k_{B1} > \sim 40$ N/m), the hydration forces are essentially negligible. The nonlinearity of the response is governed by the ratio of cantilever stiffness to sample stiffness as in Refs. 19, 20, and 22. Thus, increasing cantilever stiffness decreases the nonlinearity.

The simulations in Figs. 13(a)–13(c) fall into the first regime. Figure 13(d) shows a case where the stiffness has been increased substantially. In this case, we see that the nonlinearity is less pronounced: no nonlinear jumps and somewhat reduced superharmonics. This case falls into the second regime.

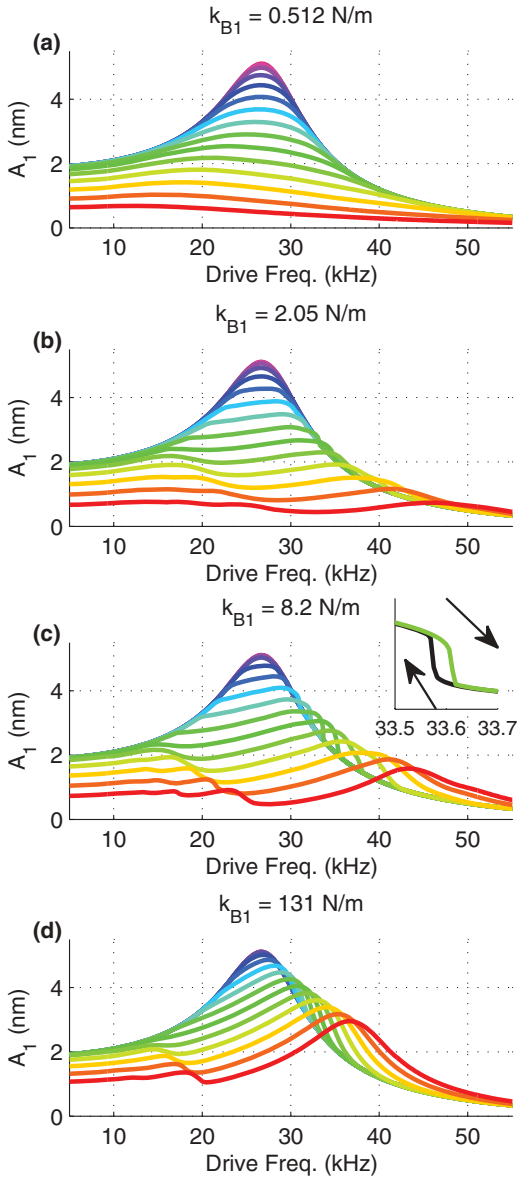


FIG. 13. (Color online) The effect of stiffness on the response. The parameters are the same as in Table II (cantilever A on mica) except $F_{B2}/F_{B1} = 1$ and the stiffness $k_{B1}$ is varied (the ratios $k_{B2}/k_{B1}$ and $k_{B3}/k_{B1}$ are kept constant). The inset in (c) compares a sweep up and a sweep down at $Z = 1.5$ nm.

### E. Effect of free amplitude on the nonlinear response

Parameter studies on the effects of free amplitude are given in the Supplemental Material.[33] The results are as expected from previous studies.[19–22,24] Briefly, larger free amplitude leads to more pronounced nonlinear features. For very small free amplitudes ($A_{\text{init}} < \sim 0.5$ nm for the parameters in Table II), the tip may not have enough force to "push through" the hydration layers to the sample, in which case imaging resolution will not be optimal.[21]

### F. Effect of sample stiffness on the nonlinear response

Based on simulations where the sample modulus is changed from 60 to 0.6 GPa while keeping hydration forces constant, we find that a softer sample leads to less energy transferred to higher harmonics and higher eigenmodes, and thus a less pronounced nonlinear result. Figures for these simulations are in the Supplemental Material.[33]

## VI. DISCUSSION: POTENTIAL APPLICATIONS OF THE NONLINEAR RESPONSE

We have thus far focused on the physics of AFM microcantilevers oscillating at liquid-solid interfaces. Here, we examine some potential practical benefits of the observations. The presence of superharmonic resonances immediately suggests the possibility of a new imaging mode. Multiple authors have suggested using higher harmonics of the cantilever deflection signal in order to gain more information about the sample. For example, Ref. 73 suggests to combine the mean deflection, first harmonic, and second harmonic in order to determine local elastic properties. One difficulty with higher-harmonic imaging, however, is that the amplitudes of the higher harmonics are often small, leading to poor signal-to-noise ratio. However, if the drive frequency is chosen to be a frequency near a superharmonic resonance, then $A_2$ will be significantly enhanced (already been suggested by Ref. 74 for operation in air). This may allow for superior determination of material properties. Reference 20 has shown the use of higher-harmonics imaging in liquids for improved compositional contrast. This work suggests that the contrast in this method could be optimized by choosing the excitation frequency and set point near the point of maximum energy transfer to higher eigenmodes [e.g., the point "A" in Fig. 9(g)].

Finally, per the discussion in Sec. IV E, the energy dissipation in the hydration layers (or into the underlying sample) is often a quantity of interest. However, the energy transfer from the driving frequency to higher harmonics/higher eigenmodes can complicate the experimental study of energy dissipation. Methods which rely on only information from the first harmonic amplitude and phase can not distinguish between the multiple energy dissipation paths shown in Fig. 9(h). Proper study of the energy dissipation requires reconstructing the response of each eigenmode separately. This is difficult with the traditional photodiode/optical beam method because the photodiode can measure only a single degree of freedom and (at least) two degrees of freedom are required. In air/vacuum, multiple eigenmodes can be separated based on frequency because the resonance bandwidths are narrow. But, in liquids, the resonance bandwidths overlap. New AFM designs that can sense multiple degrees of freedom (e.g., multiple laser/photodiodes each focused on a different region of the cantilever) may be able to better separate the eigenmode responses and thus improve quantitative results in liquids.

## VII. CONCLUSIONS

In this work, we have presented an in-depth study of nonlinear dynamics of AFM cantilevers oscillating at the liquid-solid interface. This coupled system of a continuous oscillator in liquids interacting with nanoscale forces at the interface features a host of interesting nonlinear phenomena that have been elucidated here. A theoretical model of the nonlinear frequency response of AFM cantilevers operated in liquid environment has been presented. The model has been validated

against experimental observations, and then used to analyze the observations and study the effects of various parameters. The most important conclusions are summarized as follows:

(1) It is possible for the resonance peak to split into two distinct resonance peaks due to the nonlinear tip-sample interaction (Secs. III B 2 and IV E). The secondary resonance peak appears at approximately one-half of the main resonance peak. This effect also introduces a distinct distortion in tapping mode approach curves (Fig. 4).

(2) The tip-sample interaction force has two parts: a hydration force and a Hertz contact force (Sec. IV B). In intermittent contact on hard samples, the Hertz contact force leads to a significantly stronger nonlinearity than the hydration forces. The hydration forces smooth out the tip-sample interaction (Sec. V A).

(3) The nonlinear response is strongly influenced by which of the two types of forces is most dominant. Larger cantilever stiffness (Sec. V D) and larger free amplitudes (Sec. V E) tend to decrease the effect of the hydration forces, and therefore lead to stronger nonlinearities.

(4) Different liquid-solid interfaces exhibit different hydration/hydrophobic forces, and therefore lead to distinctly different cantilever dynamic responses (Secs. III C and V B).

(5) A higher-quality factor (Sec. V C) tends to suppress the secondary resonance peaks, but creates a significantly more nonlinear response at the primary resonance (e.g., jump phenomena).

(6) Magnetic excitation can potentially excite the second eigenmode strongly, even when driving near the first natural frequency (Secs. III B 1 and IV C). When present, this response must be taken into account to achieve quantitative results, even for linear small-amplitude AFM.

All of these results confirm previous results that AFM cantilever dynamics in liquids is qualitatively different than the dynamics in air/vacuum. We anticipate wide applicability of these results. A better understanding of the dynamics should allow better hardware designs, controllers, and imaging modes that are tailored for the unique aspects of liquid AFM. Analytical formulas and techniques for identifying and mapping material and sample properties can be improved to account for the nonlinear effects. Finally, new methods for studying solvation/hydration layers by exploiting the nonlinear dynamics may be possible.

## ACKNOWLEDGMENT

The authors would like to thank the National Science Foundation for financial support through Grant No. CMMI-0927648.

[1] T. Fukuma, Y. Ueda, S. Yoshioka, and H. Asakawa, Phys. Rev. Lett. **104**, 016101 (2010).
[2] B. Song, G. Liu, R. Xu, S. Yin, Z. Wang, and X. Zhang, Langmuir **24**, 3734 (2008).
[3] A. Kueng, C. Kranz, B. Mizaikoff, A. Lugstein, and E. Bertagnolli, Appl. Phys. Lett. **82**, 1592 (2003).
[4] A. Raman, R. Reifenberger, J. Melcher, and R. Tung, *Noncontact Atomic Force Microscopy* (Springer, Berlin, 2009), Chap. 18.
[5] R. García and A. S. Paulo, Phys. Rev. B **60**, 4961 (1999).
[6] M. Koltypin, Y. S. Cohen, B. Markovsky, Y. Cohen, and D. Aurbach, Electrochem. Commun. **4**, 17 (2002).
[7] M. Delcea, S. Schmidt, R. Palankar, P. Fernandes, A. Fery, H. Möhwald, and A. Skirtach, Small **6**, 2858 (2010).
[8] A. Verdaguer, G. M. Sacha, H. Bluhm, and M. Salmeron, Chem. Rev. **106**, 1478 (2006).
[9] E. Wutscher and F. Giessibl, Rev. Sci. Instrum. **82**, 093703 (2011).
[10] P. K. Hansma, J. P. Cleveland, M. Radmacher, D. A. Walters, P. E. Hillner, M. Bezanilla, M. Fritz, D. Vie, H. G. Hansma, C. B. Prater, J. Massie, L. Fukunaga, J. Gurley, and V. Elings, Appl. Phys. Lett. **64**, 1738 (1994).
[11] H. J. Butt, K. Graf, and M. Kappl, *Physics and Chemistry of Interfaces* (Wiley, Weinheim, 2003).
[12] J. Israelachvili, *Intermolecular and Surface Forces*, 2nd ed. (Academic, London, 1992).
[13] J. Melcher, X. Xu, and A. Raman, Appl. Phys. Lett. **93**, 93111 (2008).
[14] S. Basak and A. Raman, Appl. Phys. Lett. **91**, 064107 (2007).
[15] S. J. T. van Noort, O. H. Willemsen, K. O. van der Werf, B. G. de Grooth, and J. Greve, Langmuir **15**, 7101 (1999).
[16] D. Sarid, J. Chen, and R. K. Workman, Comput. Mater. Sci. **3**, 475 (1995).
[17] G. Y. Chen, R. J. Warmack, P. I. Oden, and T. Thundat, J. Vac. Sci. Technol. B **14**, 1313 (1996).
[18] J. Legleiter and T. Kowalewski, Appl. Phys. Lett. **87**, 163120 (2005).
[19] J. Melcher, C. Carrasco, X. Xu, J. L. Carrascosa, J. Gómez-Herrero, P. J. D. Pablo, and A. Raman, Proc. Natl. Acad. Sci. USA **106**, 13655 (2009).
[20] X. Xu, J. Melcher, S. Basak, R. Reifenberger, and A. Raman, Phys. Rev. Lett. **102**, 060801 (2009).
[21] D. Martinez-Martin, C. Carrasco, M. Hernando-Perez, P. J. de Pablo, J. Gomez-Herrero, R. Perez, M. Mateu, J. L. Carrascosa, D. Kiracofe, J. Melcher, and A. Raman, PLoS ONE **7**, e30204 (2012).
[22] D. Kiracofe and A. Raman, J. Appl. Phys. **108**, 034320 (2010).
[23] M. Lantz, Y. Z. Liu, X. D. Cui, H. Tokumoto, and S. M. Lindsay, Surf. Interface Anal. **27**, 354 (1999).
[24] D. Niu, Y. Chen, and W. Huang, Meas. Sci. Technol. **21**, 105503 (2010).
[25] M. H. Korayem and N. Ebrahimi, J. Appl. Phys. **109**, 084301 (2011).
[26] Y. Wu, C. Gupta, and M. A. Shannon, Langmuir **24**, 10817 (2008).
[27] D. J. Müller, D. Fotiadis, S. Scheuring, S. A. Müller, and A. Engel, Biophys. J. **76**, 1101 (1999).
[28] A. Labuda, K. Kobayashi, D. Kiracofe, K. Suzuki, P. Grütter, and H. Yamada, AIP Advances **1**, 022136 (2011).
[29] S. Jeffery, P. M. Hoffmann, J. B. Pethica, C. Ramanujan, H. O. Özer, and A. Oral, Phys. Rev. B **70**, 054114 (2004).
[30] W. Han and S. M. Lindsay, Appl. Phys. Lett. **69**, 4111 (1996).
[31] S. Crittenden, A. Raman, and R. Reifenberger, Phys. Rev. B **72**, 235422 (2005).
[32] A similar looking secondary peak appears to have been predicted in some of the simulations in Ref. 24. However, it does not appear

in their experimental results and there is no discussion of the phenomena in that work.

[33]See Supplemental Material at http://link.aps.org/supplemental/10.1103/PhysRevB.86.205405 for additional experimental data, simulation results, and parameter studies, as well as discussions on hydrodynamic effects and magnetic forcing at the second eigenmode.

[34]J. E. Sader, J. Appl. Phys. **84**, 64 (1998).

[35]D. Kiracofe and A. Raman, J. Appl. Phys. **107**, 3506 (2010).

[36]R. Proksch, T. E. Schäffer, J. P. Cleveland, R. C. Callahan, and M. B. Viani, Nanotechnology **15**, 1344 (2004).

[37]T. E. Schäffer, J. P. Cleveland, F. Ohnesorge, D. A. Walters, and P. K. Hansma, J. Appl. Phys. **80**, 3622 (1996).

[38]S. de Beer, D. van den Ende, and F. Mugele, J. Phys.: Condens. Matter **23**, 112206 (2011).

[39]X. Xu and A. Raman, J. Appl. Phys. **102**, 034303 (2007).

[40]D. Kiracofe and A. Raman, Nanotechnology **22**, 485502 (2011).

[41]P. J. Wei, Y. X. Shen, T. F. Lin, and J. F. Lin, Micro. Nano Lett IET **6**, 9 (2011).

[42]S. I. Lee, S. W. Howell, A. Raman, and R. Reifenberger, Phys. Rev. B **66**, 115409 (2002).

[43]R. Proksch, Appl. Phys. Lett. **89**, 113121 (2006).

[44]Note that the small peak in $A_2$ at 36.5 kHz (marked with an arrow in Fig. 6) is an artifact due to the saturation of the solenoid core used for magnetic excitation.

[45]https://nanohub.org/tools/veda

[46]D. Kiracofe, J. Melcher, and A. Raman, Rev. Sci. Instrum. **83**, 013702 (2012).

[47]J. Melcher, S. Hu, and A. Raman, Rev. Sci. Instrum. **79**, 061301 (2008).

[48]Properly speaking, the added mass and added viscosity are frequency dependent. However, for the experimental conditions considered in this work, the dependence is weak. Additional details can be found in the Supplemental Material (Ref. 33).

[49]J. Melcher, S. Hu, and A. Raman, Appl. Phys. Lett. **91**, 53101 (2007).

[50]$\psi$ is chosen such that $\psi_i(L) = 1$ so that the modal coordinates are the deflection of cantilever at the free end. This scaling is important because it allows the calibrated stiffnesses of the eigenmodes to be incorporated directly into the model (Ref. 49).

[51]For most of the simulations presented here, $N = 2$ and $N = 3$ are virtually identical. The simulations discussed in Sec. V A that include Hertz contact forces only and no hydration forces do show some differences between $N = 2$ and 3.

[52]J. E. Sader, J. W. M. Chon, and P. Mulvaney, Rev. Sci. Instrum. **70**, 3967 (1999).

[53]D. Kiracofe, J. Melcher, and A. Raman, *Atomic Force Microscopy in Liquids: Biological Applications* (Wiley, New York, 2012), pp. 121–156.

[54]M. Penedo and M. Luna (unpublished).

[55]M. J. Higgins, R. Proksch, J. E. Sader, M. Polcik, S. Mc Endoo, J. P. Cleveland, and S. P. Jarvis, Rev. Sci. Instrum. **77**, 013701 (2006).

[56]G. B. Kaggwa, J. I. Kilpatrick, J. E. Sader, and S. P. Jarvis, Appl. Phys. Lett. **93**, 011909 (2008).

[57]S. deBeer, W. K. Otter, D. Ende, W. J. Briels, and F. Mugele, Europhys. Lett. **97**, 46001 (2012).

[58]S. deBeer, D. Ende, and F. Mugele, Nanotechnology **21**, 325703 (2010).

[59]S. J. O'Shea and M. E. Welland, Langmuir **14**, 4186 (1998).

[60]T. Fukuma, M. J. Higgins, and S. P. Jarvis, Biophys. J. **92**, 3603 (2007).

[61]K. L. Johnson, *Contact Mechanics* (Cambridge University Press, Cambridge, UK, 1985).

[62]For some samples, the attractive forces may not be negligible and thus the Derjaguin-Muller-Toporov (DMT) model may be more appropriate than the Hertz model. However, a net attractive force in Eq. (6) can also be accomplished by taking $p_h$ to be negative in Eq. (3). Therefore, a fair amount of generality is retained in Eq. (6) even without the DMT model.

[63]S. J. O'Shea, M. A. Lantz, and H. Tokumoto, Langmuir **15**, 922 (1999).

[64]E. T. Herruzo and R. García, Appl. Phys. Lett. **91**, 143113 (2007).

[65]A. H. Nayfeh and D. T. Mook, *Nonlinear Oscillations* (Wiley, New York, 1979).

[66]Subharmonic resonances, a response at a lower frequency than the excitation frequency, are also possible in liquid AFM (Ref. 22).

[67]A. Payam, J. Ramos, and R. Garcia, ACS Nano **6**, 4663 (2012).

[68]Also note that the work of Ref. 13 on multiple impact regimes did not include the effects of hydration forces. By smoothing out the tip-sample interaction force, the hydration layers make multiple impacts less likely to occur than Ref. 13 predicted.

[69]T.-D. Li, J. Gao, R. Szoszkiewicz, U. Landman, and E. Riedo, Phys. Rev. B **75**, 115415 (2007).

[70]C. Sendner, D. Horinek, L. Bocquet, and R. R. Netz, Langmuir **25**, 10768 (2009).

[71]S. Sadewasser and T. Glatzel, Phys. Rev. Lett. **98**, 269701 (2007).

[72]To some degree, one can increase the quality factor of the cantilever by immersing it in a liquid with a lower viscosity. Some results for acetone are shown in the Supplemental Material (Ref. 33).

[73]A. Raman, S. Trigueros, A. Cartagena, A. P. Z. Stevenson, M. Susilo, E. Nauman, and S. A. Contera, Nat. Nanotechnol. **6**, 809 (2011).

[74]M. Balantekin and A. Atalar, Phys. Rev. B **71**, 125416 (2005).